Theoretical study on the atmospheric degradation mechanism and subsequent products of E,E-2,4-hexadienal with hydroxyl radical

Yanan Sun[1], Junfang Yao[1], Yizhen Tang[2], Yunju Zhang[3], Wenzhong Wu[4], Jingyu Sun[1*]

[1] *Hubei Key Laboratory of Pollutant Analysis & Reuse Technology*, *College of Chemistry and Chemical Engineering, Hubei Normal University, Cihu Road 11, Huangshi, Hubei, 435002, P. R. China*

[2]*School of Environmental and municipal Engineering, Qingdao University of Technology , Fushun Road 11. Qingdao, Shandong, 266033, P.R. China.*

[3]*Key Laboratory of Photoinduced Functional Materials, Mianyang Normal University, Mianyang, Sichuan, 621000, P. R. China*

[4]*College of Foreign Languages, Hubei Normal University, Cihu Road 11, Huangshi, Hubei 435002, P. R. China*

[1] Corresponding author. Email address: sunjy@hbnu.edu.cn Tel.:; Fax: 0714-6515602

Abstract: E,E-2,4-hexadienal is probably a precursor of secondary organic aerosol (SOA) and plays an important role in the atmospheric chemistry. Its main degradation routs are the reactions with OH, Cl, NO_3 as well as photolysis. Atmospheric hydroxyl radical, as the most important oxidant, generally controls the removal of volatile organic compounds (VOCs) in the atmosphere. Thus, the quantum chemical calculations are used to investigate the reaction mechanism of E,E-2,4-hexadienal with hydroxyl radical, which would give better understanding for the main degradation products. The reaction paths of E,E-2,4-hexadienal with OH radical have been calculated accurately at the BMC-CCSD//M06-2X/6-311G (d, p) level at atmospheric pressure and room temperature. There are six hydrogen abstraction and four carbon addition paths at the first stages of this reaction. Due to the low energy barrier and reaction exotherm, the ten paths would contribute to the total reaction. Furthermore, the peroxy (RO_2) and alkoxy (RO) radicals from the most important adduct IM1($CH_3CHOHCHCH=CHCHO$) would be formed in the atmospheric environment. The reaction mechanism of the peroxy radical ($CH_3CHOHCHO_2CH=CHCHO$) with NO, NO_2, HO_2, and self-reaction have been studied by using the same quantum chemical methods. And the reaction paths of alkoxy radical ($CH_3CHOHCHOCH=CHCHO$) have been also originally studied. The subsequent reactions play a key role in the cycling of atmospheric radicals, production of ozone, and SOA formation. What's more, the reaction mechanism of this study accords with the reported experimental observations.

Keywords: E,E-2,4-hexadienal, VOCs, Hydroxyl radical, Peroxy radical, Quantum chemical calculations, Degradation mechanism

1. Introduction

Volatile organic compounds (VOCs) generally participate in the formation of secondary aerosols and affect the regional ozone and PM2.5 pollution[1,2]. Oxygen-containing volatile organic compounds (OVOCs), a subset of VOCs, are the intermediates of photochemical reactions in the atmosphere[3,4]. As we know, OVOCs are mainly composed of aldehydes, ketones, ethers, acids, esters and their derivant. They are easy to be degraded by oxidation reactions with OH, Cl, and NO_3 in the atmosphere[5,6], in which the most important degradation route is reaction with OH radical. OVOCs with Cl atoms reactions are fast especially in coastal areas where high concentration peaks are discovered. In the case of reactions with NO_3 radical, they play a determinant role during night time. In brief, the studies of the degradation mechanism of OVOCs can provide new insight into environmental impacts[7].

The unsaturated aldehydes play a unique role in atmospheric sciences due to their large constituent in OVOCs and high reactivity. They are emitted to the atmosphere from anthropogenic resources such as industrial, vehicle and domestic heating and from vegetation emission such as the wounded and cut plants[8,9]. E, E-2,4-hexadienal, an unsaturated C_6 aldehyde, is used as food additives and chemical intermediates, which lead to its release into the atmosphere. This compound are also emitted to atmosphere from the wounded plants[10]. Furthermore, its emission may contribute to the formation of other oxygenated species and secondary organic aerosols (SOAs). For instance, Zhao et al. studied uptake of 2,4-hexadienal by liquid H_2SO_4 over the temperature range of 250-298 K and acidic range of 60-85 wt%[11]. Henry's law solubility constant (H^*) was determined and irreversible reactive uptake was observed for 2,4-hexadienal. The formation of unsaturated polymers may explain

the irreversible loss of 2,4-hexadienal in sulfuric acid interface. This heterogeneous interaction is important for SOA formation in the upper troposphere.

In the case of homogeneous (gas-phase) reactions of E,E-2,4-hexadienal only three studies have been reported. The photolytic processes of E,E-2,4-hexadienal have been investigated[12]. Their results suggest that the photolytic reaction is reversible. Although photolysis of this compound is supposed to be an important degradation pathways for E,E-2,4-hexadienal, this reversible nature means that the removal pathways of this compound should be reactions with OH, NO_3 radicals and Cl atoms. The rate coefficients have been determined for the reaction of E,E-2,4-hexadienal with OH, NO_3 radicals and Cl atoms at atmospheric pressure and room temperature[13]. Also, the photolysis coefficient were obtained. These results show that the main sink routes for E,E-2,4-hexadienal are the reactions with OH radicals and sunlight during day time and its reaction with NO_3 radicals at night, with the atmospheric lifetimes of 4, 2.5 and 0.4 hours, respectively. It is worth noting that reaction products of E,E-2,4-hexadienal with OH, NO_3 radicals and Cl atoms have been analyzed[14]. According to the identified products, the reaction mechanism was proposed. All of results present a mechanism that the first stages occur addition of an atom or radical to the double bond of E,E-2,4-hexadienal and the aldehydic and hydrocarbyl hydrogen abstraction. An example of the reaction mechanism of E,E-2,4-hexadienal with OH radical is as follows:

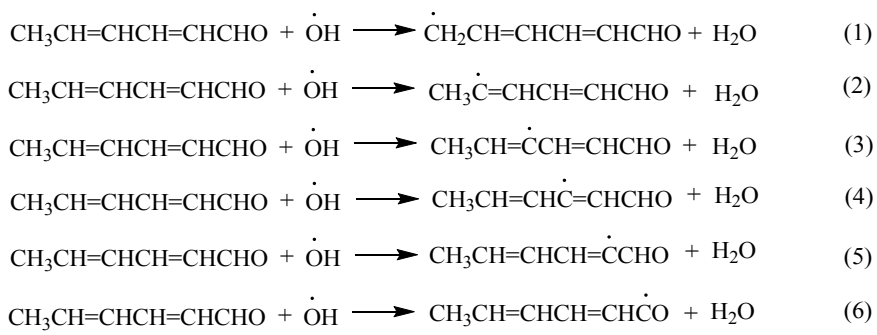

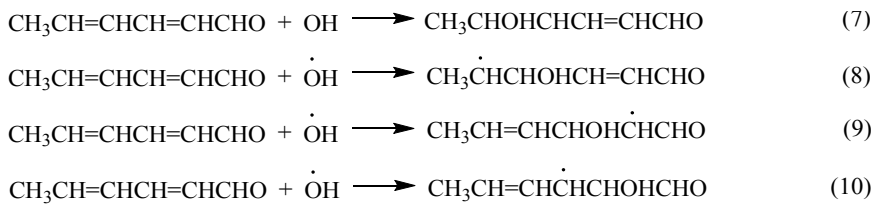

$$CH_3CH=CHCH=CHCHO + OH \longrightarrow CH_3CHOHCHCH=CHCHO \quad (7)$$

$$CH_3CH=CHCH=CHCHO + \dot{O}H \longrightarrow CH_3\dot{C}HCHOHCH=CHCHO \quad (8)$$

$$CH_3CH=CHCH=CHCHO + \dot{O}H \longrightarrow CH_3CH=CHCHOH\dot{C}HCHO \quad (9)$$

$$CH_3CH=CHCH=CHCHO + \dot{O}H \longrightarrow CH_3CH=CH\dot{C}HCHOHCHO \quad (10)$$

For the most important intermediate $CH_3CHOHCHCH=CHCHO$, the critical process is the addition of O_2 in which the corresponding peroxy radical ($CH_3CHOHCHO_2CH=CHCHO$) is produced. It is known that the peroxy radicals represent key intermediates in the atmospheric oxidation of VOCs. Their subsequent oxidation influences the level of ozone, the formation of SOAs, and the cycles of reactive radicals. Hence, the typical reactions of peroxy radicals with NO_x (NO and NO_2), HO_2 and self-reaction have been emphasised[15]. Summarizing these results, $CH_3CHOHCHO_2CH=CHCHO$ would react with NO, NO_2, HO_2 and self-reaction in the atmosphere. Although some degradation products of the reaction of E,E-2,4-hexadienal with OH radicals have been discussed in the cited literature, the intensive reaction mechanism is not well-known. The preferred sites of addition and abstraction for E,E-2,4-hexadienal are still puzzled scientists. Meanwhile, the main product pathways are also ambiguous in the complicated environment. Thus, in this work, the detailed reaction mechanism of E,E-2,4-hexadienal with OH radical has been explored, including the first stages initiated and subsequent oxidation. The degradation paths of RO_2 ($CH_3CHOHCHO_2CH=CHCHO$) radical with NO, NO_2, HO_2, self-reaction, and the relevant reactions of the abundant RO ($CH_3CHOHCHOCH=CHCHO$) radical are calculated. Expectantly, theoretical results can explain previous experimental phenomenon and provide guidance for future experimental measurement.

2. Computational methods

The M06-2X functional[16]combined with the triple-ξ basis set 6-311G (d, p) [17]was used to optimize the geometric structure of all standing points (reactants, complexes, transition states, intermediates and products) and to analyze the vibration frequencies. The M06-2X has been recommended for giving accurate results such as thermochemical and kinetic data[18-20]. The intermediates and transition states are determined by frequency analysis (number of imaginary frequencies, NIMAG, 0 for minima and 1 for transition states), and the final reactants and products connected by transition states are determined by internal reaction coordinate (IRC) method[21,22]. In order to obtain reliable potential energy surface of these reactions, high-level BMC-CCSD method was used for energy calculations. The principle of BMC-CCSD is coupled cluster theory, which includes single and double excitations[23]. The expression of the combinational algorithm BMC-CCSD is described below:

E(BMC-CCSD)=E(HF/6-31B(d))+1.06047423Δ(HF/MG3|6-31B(d))

+1.09791Δ(MP2|HF/6-31B(d))+1.33574Δ(MP2|HF/MG3/6-31B(d))

+0.90363Δ(MP4(DQ)|MP2/6-31B(d))+1.55622Δ(CCSD|MP4(DQ)/6-31B(d))+

ZPE+Eso

Where ΔE(L2|L1/B)≡E(L2/B)-E(L1/B);

ΔE(L/B2|B1)≡E(L/B2)-E(L/B1)

The BMC-CCSD method has been proved in the accuracy of reaction energies. For example, in the reactions of aliphatic aldehyde and NO_2, BMC-CCSD method has obtained accurate potential energy surfaces[24,25]. Therefore, the M06-2X and BMC-CCSD calculations are carried out using the Gaussian09 program[26].

3. Results and discussion

A reaction mechanism for degradation of E,E-2,4-hexadienal with OH radical

would gain a better understanding for high-weight unsaturated aldehydes in the atmospheric chemistry. In the following sections, we will separately discuss the first stage of this reaction and further degradation reactions of the key radicals (RO_2 and RO) with NO, NO_2, HO_2, and self-reaction. The optimized structures of complexes, stable intermediates and transition states are shown in Figure 1. The relative energies and reaction enthalpy are summarized in Table 1. The vibrational frequencies of all species are shown in Table S1 (supporting information). And the potential energy surfaces for these reactions are described in Figure 2.

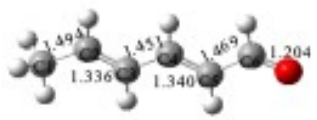

R

OH

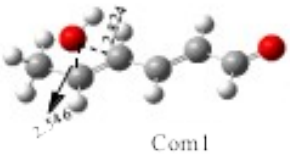

Com1

Com2

TS1

TS2

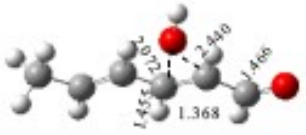

TS3

TS4

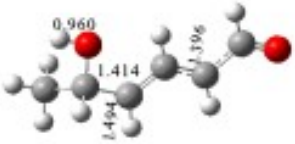

IM1

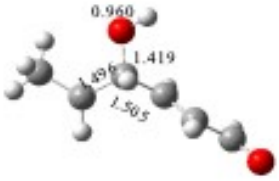

IM2

IM3

IM4

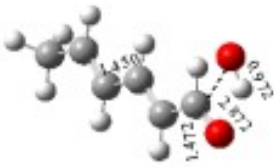

CR1

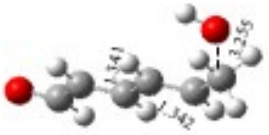

CR2

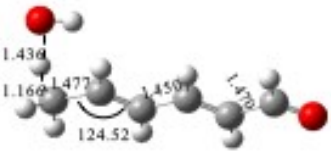

HTS1

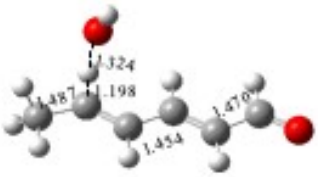

HTS2

HTS3

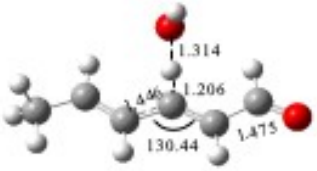

HTS4

HTS5

136

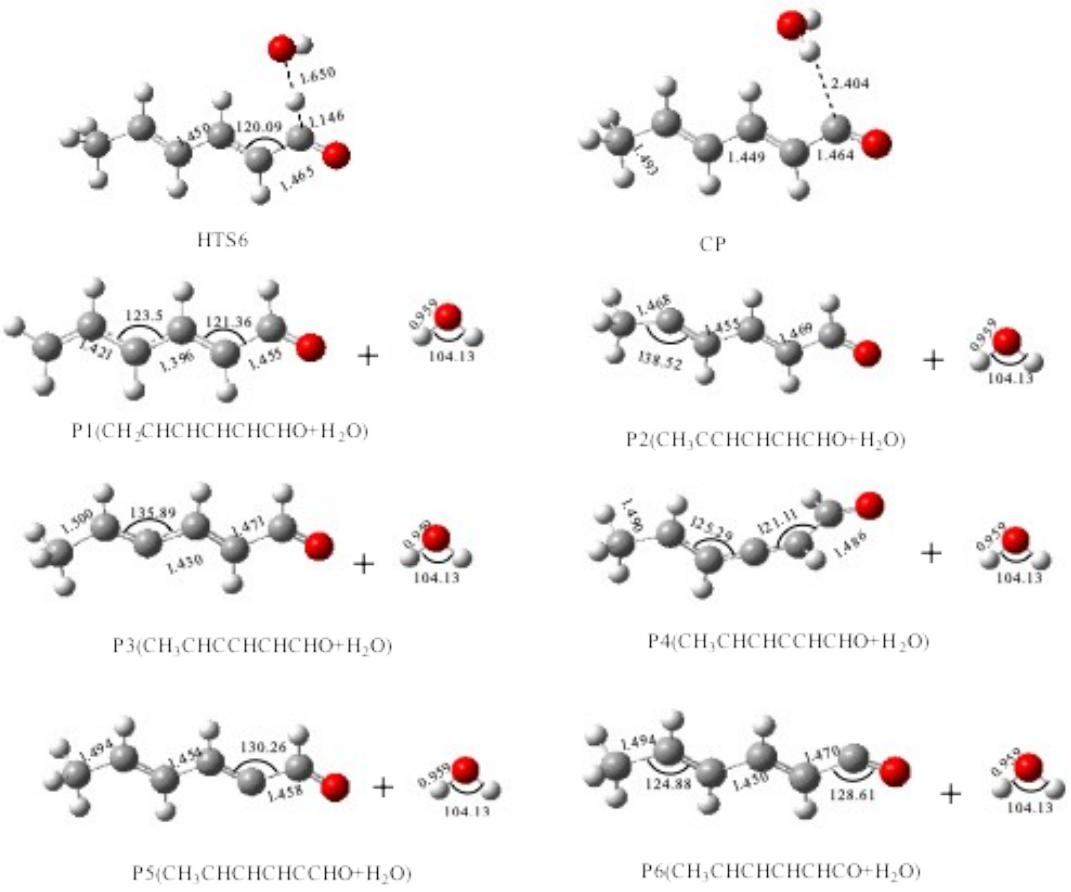
1.650
1.146
120.09
1.459
1.465
HTS6
2.404
1.493
1.449
1.464
CP
123.5
121.36
1.421
1.396
1.455
0.959
104.13
P1(CH2CHCHCHCHCHO+H2O)
1.468
1.455
1.469
138.52
0.959
104.13
P2(CH3CCHCHCHCHO+H2O)
1.500
135.89
1.471
1.430
0.959
104.13
P3(CH3CHCCHCHCHO+H2O)
1.498
125.29
121.11
1.486
0.959
104.13
P4(CH3CHCHCCHCHO+H2O)
1.694
1.454
130.26
1.458
0.959
104.13
P5(CH3CHCHCHCCHO+H2O)
1.494
124.88
1.450
1.470
128.61
0.959
104.13
P6(CH3CHCHCHCHCO+H2O)

(a)

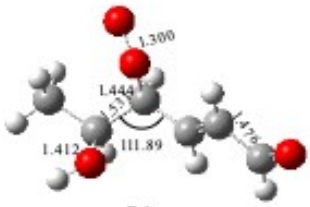

R1

NO

Trans-RO_2NO

Cis-RO_2NO

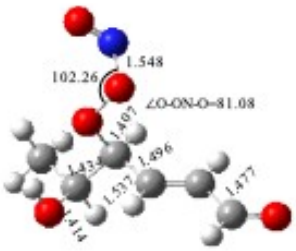

TS-1

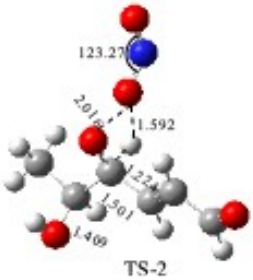

TS-2

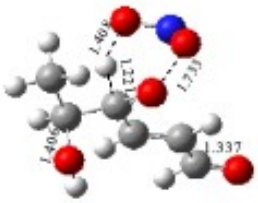

TS-3

TS-4

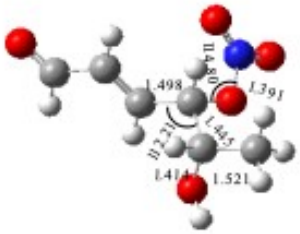

$RONO_2$

RO

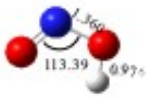

HONO

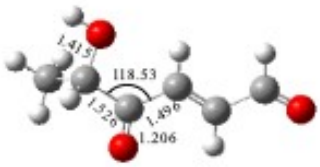

R=O

139

140 (b)

NO_2

RO_2NO_2

TS-5

HNO_3

141

142 (c)

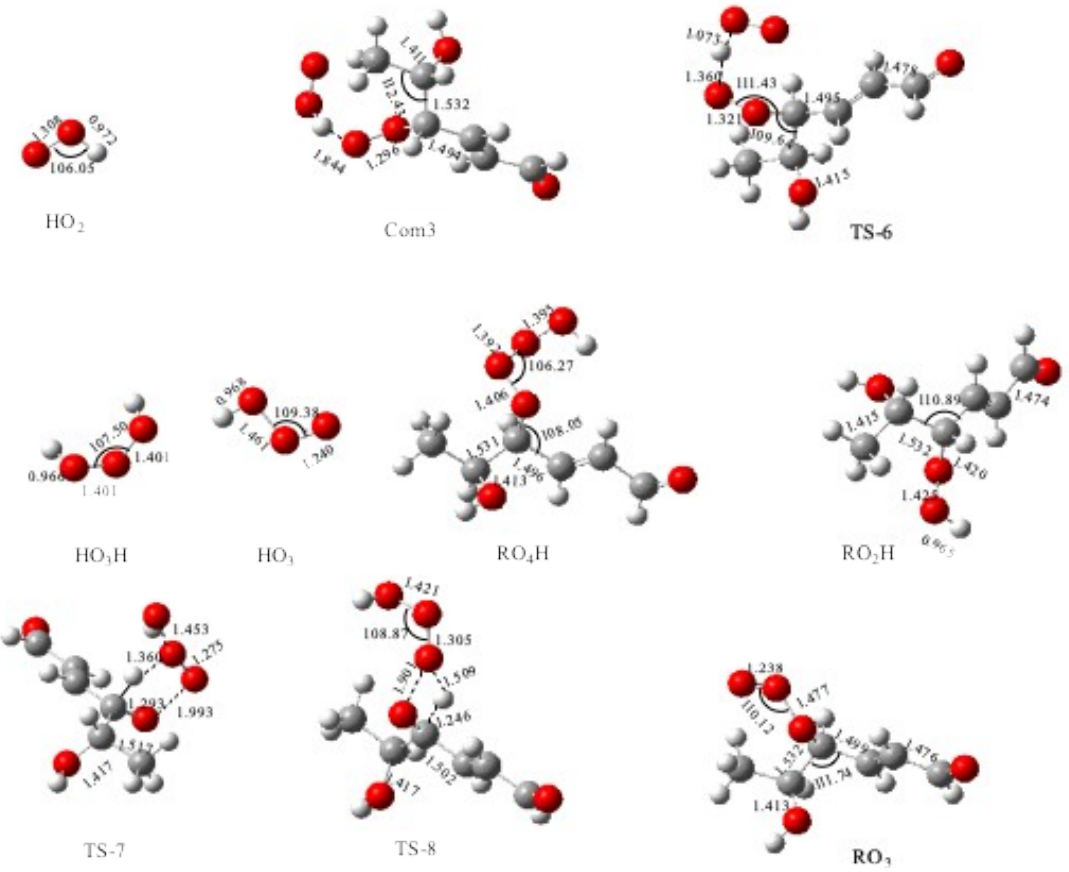

143

144 (d)

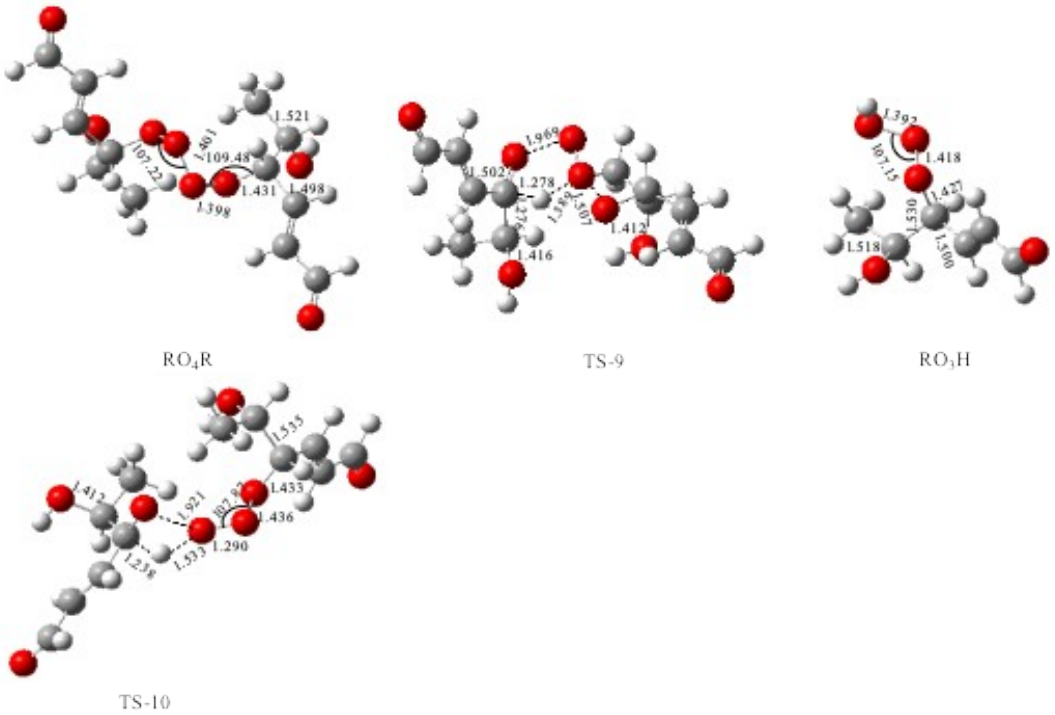
1.521
107.22
109.48
1.431
1.498
1.398
RO4R
1.969
1.502
1.278
1.412
1.416
TS-9
1.418
1.530
1.518
1.500
RO3H
1.535
1.412
1.921
1.433
1.436
1.290
1.533
1.258
TS-10

145

146 (e)

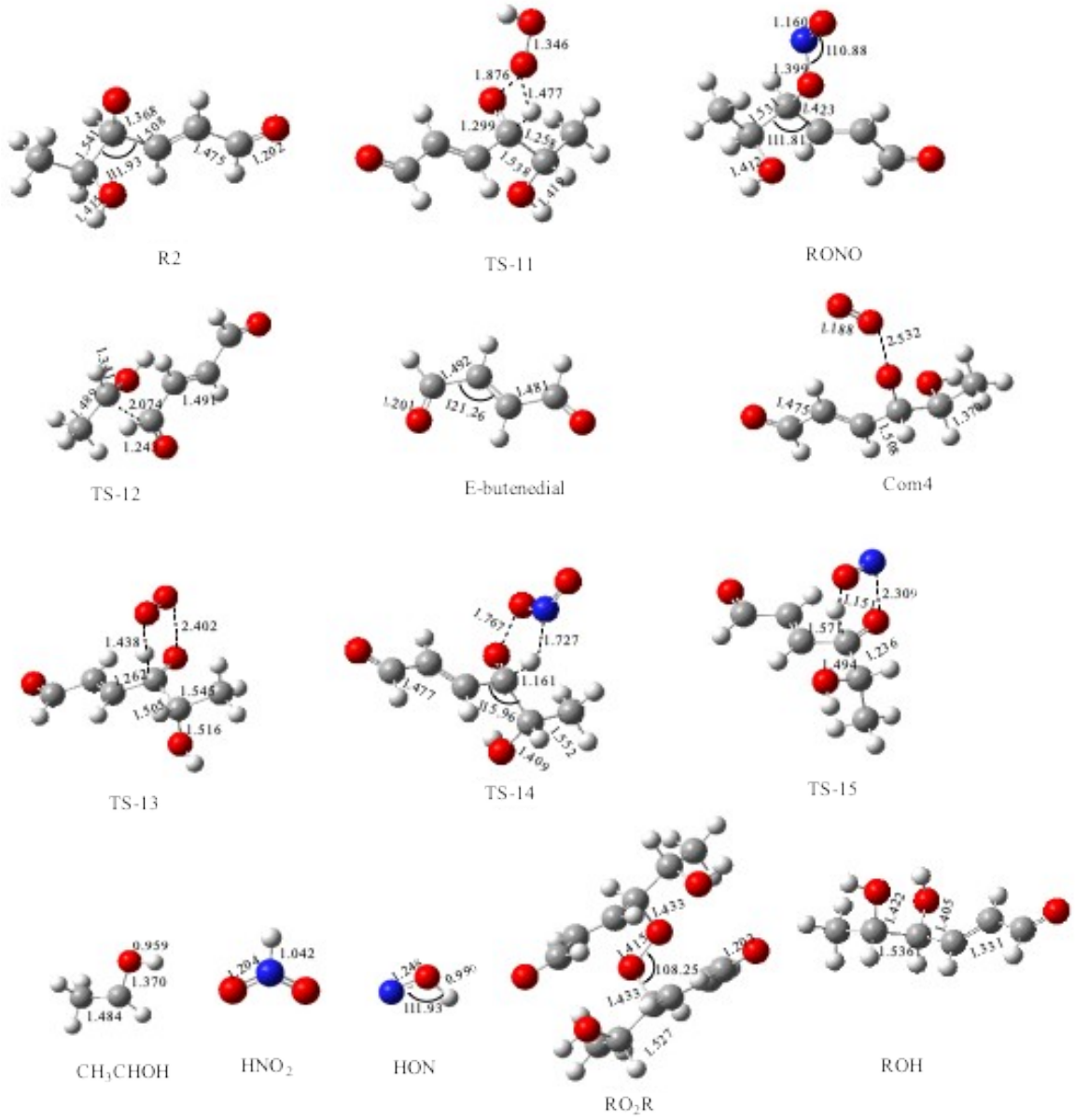

147

148 (f)

149 Figure1 The geometric structures of the reactants, complexes, transition states,

150 intermediates, and products in this study at the M06-2X/6-311G(d,p) level (distance in

151 Å and angles in degree). More specifically, (a) Structures for the first stage of

152 hydrogen abstraction and C-addition reaction paths. (b) Structures for peroxy radical

153 (R1) + NO reaction path. (c) Structures for the R1 + NO_2 reaction path. (d) Structures

154 for the R1+ HO_2 reaction path. (e) Structures for the R1 self-reaction path. (f)

155 Structures of subsequent reactions for alkoxy radical (R2).

156 Table 1 Relative energy and enthalpy obtained at two levels of M06-2X/6-311G (d, p)

157 and BMC-CCSD//M06-2X/6-311G (d, p) at 298 K (unit: kcal/mol)

Species	ΔE^a	ΔE^b	ΔH^b	Species	ΔE^a	ΔE^b	ΔH^b
R+OH	0	0	0	TS-6	-9.10	-4.71	-5.31
Com1	-5.26	-2.78	-2.91	$RO_2H+{}^3O_2$	-36.84	-36.32	-23.12
Com2	-4.56	-2.03	-2.16	RO_4H	-11.16	-14.21	-8.96
TS1	-3.88	-4.36	-5.33	TS-7	32.02	17.54	14.42
TS2	0.58	-2.04	-2.80	TS-8	30.61	16.01	13.96
TS3	-0.77	-2.63	-3.50	$R=O+HO_2+OH$	-27.61	-29.01	-18.67
TS4	-1.37	-2.38	-3.15	$R=O+HO_3H$	-55.18	-58.73	-40.44
IM1	-43.34	-42.00	-43.29	RO_3+OH	15.56	10.16	5.98
IM2	-24.97	-22.65	-23.64	$RO+HO_3$	9.64	7.67	3.84
IM3	-30.39	-27.56	-28.77	$RO+{}^3O_2+OH$	4.72	9.05	9.89
IM4	-38.61	-37.36	-38.59	2×R1	0	0	0
CR1	-4.56	-2.03	-2.22	RO_4R	-12.00	-16.81	-17.21
CR2	-5.26	-2.78	-2.91	TS-9	14.73	-1.82	-2.40
HTS1	0.81	-1.03	-1.66	TS-10	28.09	11.11	10.61
HTS2	1.34	1.97	1.22	$R=O+RO+HO_2$	-32.95	-31.76	-30.81
HTS3	1.50	2.27	1.54	$R=O+RO_3H$	-55.27	-58.16	-58.16
HTS4	1.14	2.49	1.80	RO_3+RO	10.23	7.41	7.46
HTS5	1.26	1.77	1.04	$2\times RO+{}^3O_2$	-0.61	6.30	7.11
HTS6	-3.37	-2.23	-2.90	$R2+NO_2$	0	0	0
CP	-32.30	-31.96	-31.77	$RONO_2$	-38.20	-45.29	-46.25

P1	-34.09	-39.83	-39.81	TS-4	2.03	-10.90	-11.88
P2	-8.09	-10.04	-9.61	TS-14	18.79	3.97	3.13
P3	-5.81	-12.43	-12.00	R=O+HONO	-65.19	-72.90	-72.96
P4	-14.32	-19.00	-18.52	R=O+HNO_2	-54.73	-65.39	-65.48
P5	-2.86	-8.78	-8.39	R2+NO	0	0	0
P6	-25.80	-30.25	-29.97	RONO	-37.51	-50.14	-51.01
R1+NO	0	0	0	TS-15	8.06	-4.68	-5.40
Trans-RO_2NO	-18.38	-23.06	-23.89	R=O+HON	9.43	-0.84	-0.71
Cis-RO_2NO	-20.37	-24.29	-25.21	TS-12	2.53	-11.39	-11.49
TS-1	-10.10	-14.08	-15.18	CH_3CHOH+ E-butenedial	5.66	-4.03	-3.20
TS-2	26.68	10.59	9.95	R2+O_2	0	0	0
TS-3	21.32	13.92	12.64	Com4	-39.95	-36.45	-36.36
TS-4	-9.86	-18.27	-19.46	TS-13	-31.12	-35.08	-35.57
RO+NO_2	-4.40	-10.46	-10.73	R=O+HO_2	-70.00	-73.66	-73.53
$RONO_2$	-50.44	-55.07	-56.19	R2+HO_2	0	0	0
R=O+HONO	-73.84	-77.33	-77.67	RO_3H	-26.90	-34.46	-35.81
R1+NO_2	0	0	0	TS-11	18.79	-1.74	-2.80
RO_2NO_2	-23.42	-24.33	-25.25	R=O+HO_2H	-70.12	-81.86	-81.82
RO+NO_3	20.65	16.46	16.29	RO_2+OH	6.08	-3.29	-2.94
TS-5	11.04	7.55	6.35	2×R2	0	0	0
R=O+HNO_3	-77.16	-77.62	-78.09	RO_2R	-38.08	-56.69	-57.34
R1+HO_2	0	0	0	ROH+R=O	-93.58	- 112.59	- 112.73
Com3	-8.43	-7.08	-4.77				

158 [a] refers to the energy at the M06-2X/6-311G (d, p) level; [b] refers to the energy and

159 enthalpy at the BMC-CCSD//M06-2X/6-311G (d, p) level.

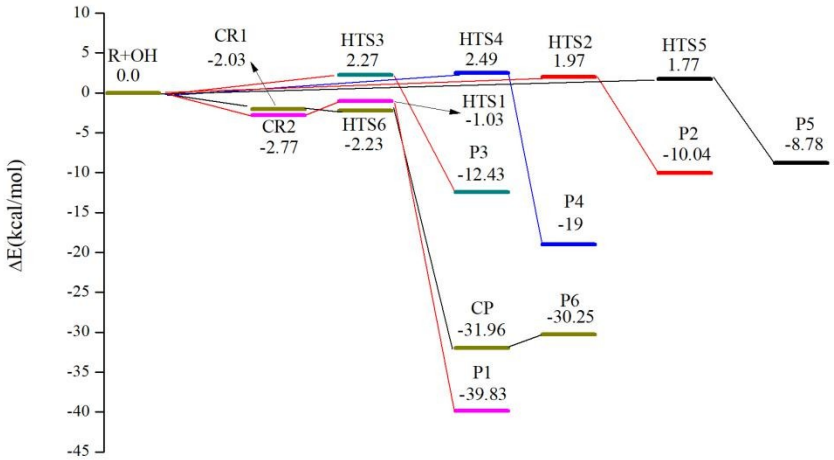

160

161 (a)

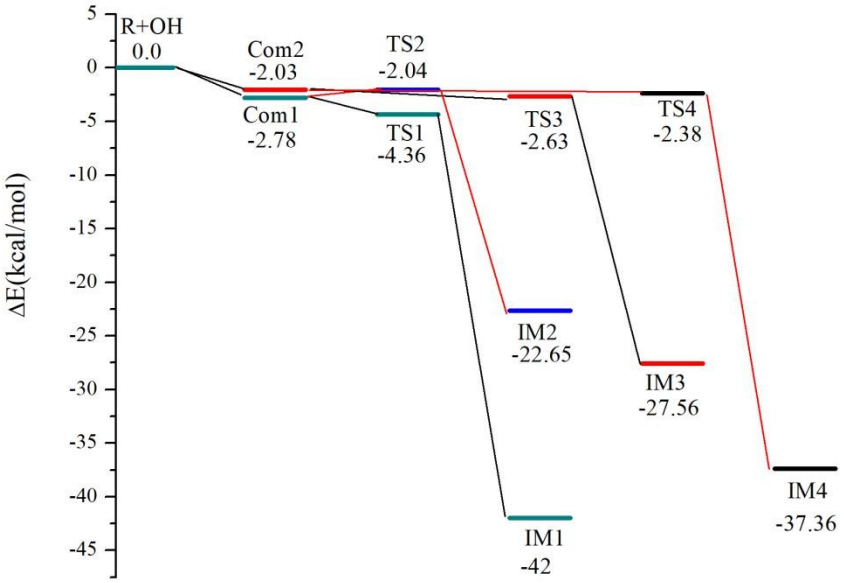

162

163 (b)

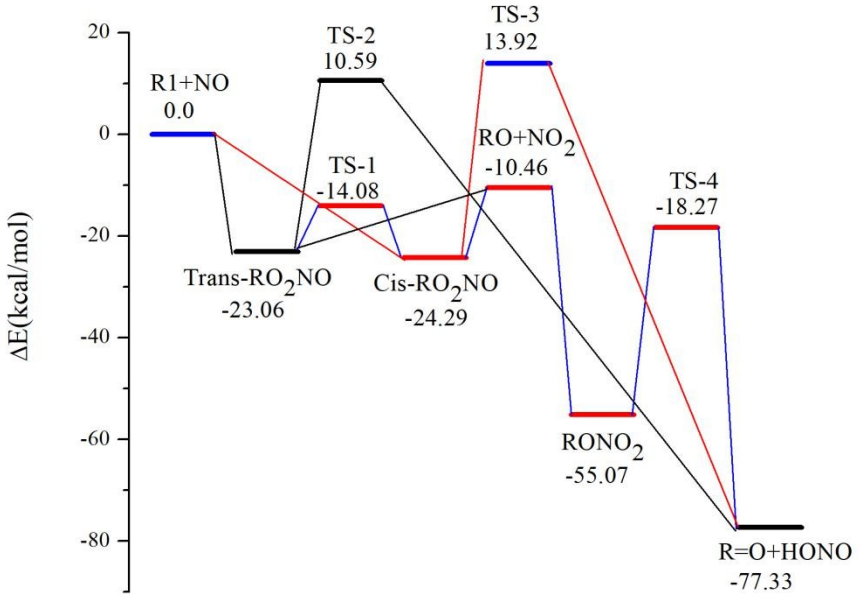

164

165 (c)

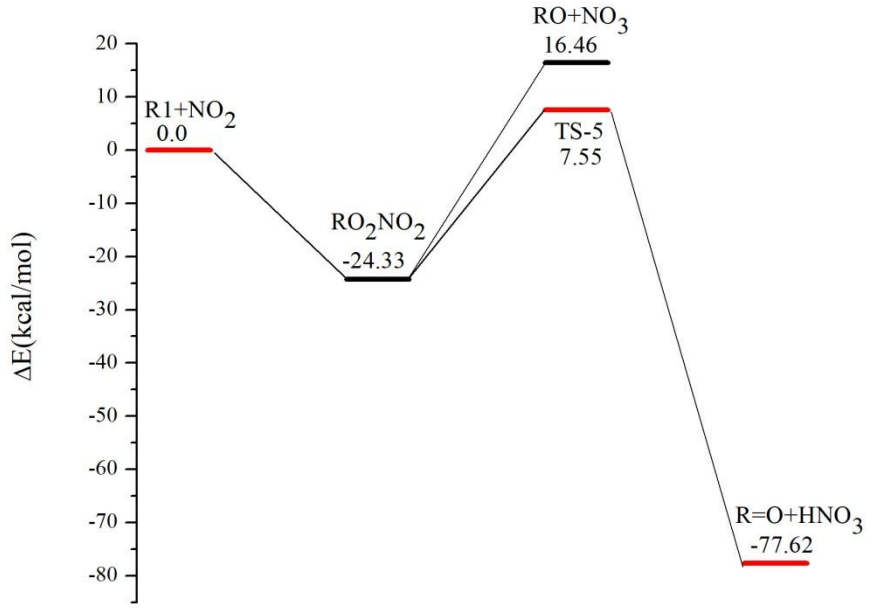

166

167 (d)

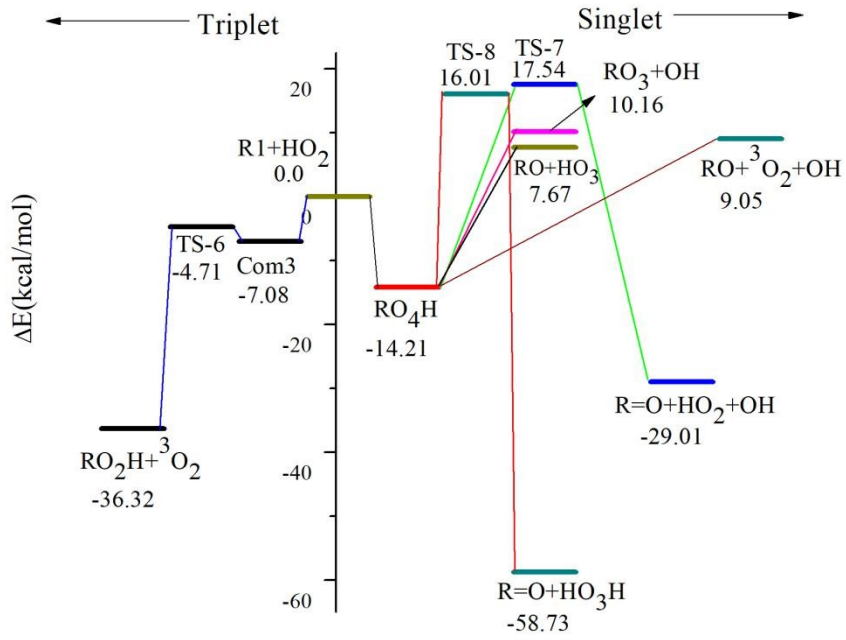

168

169 (e)

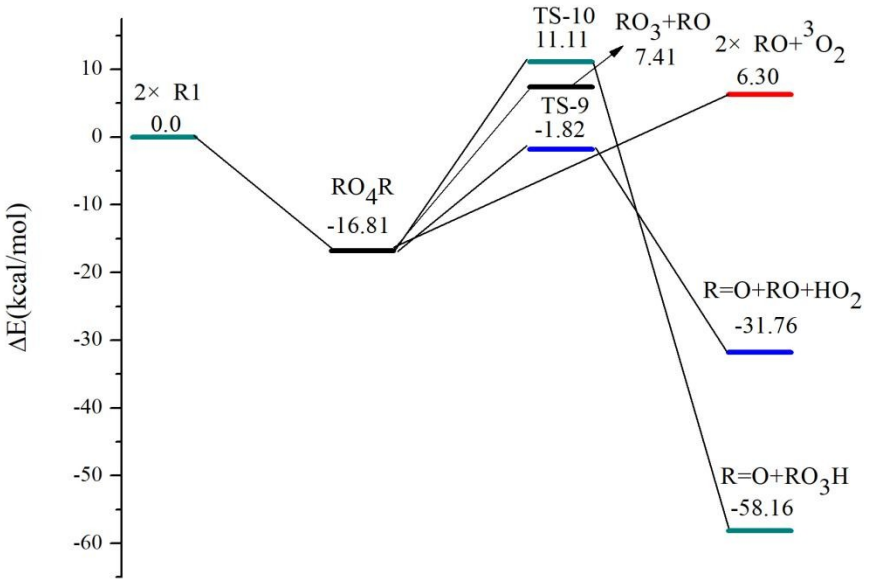

170

171 (f)

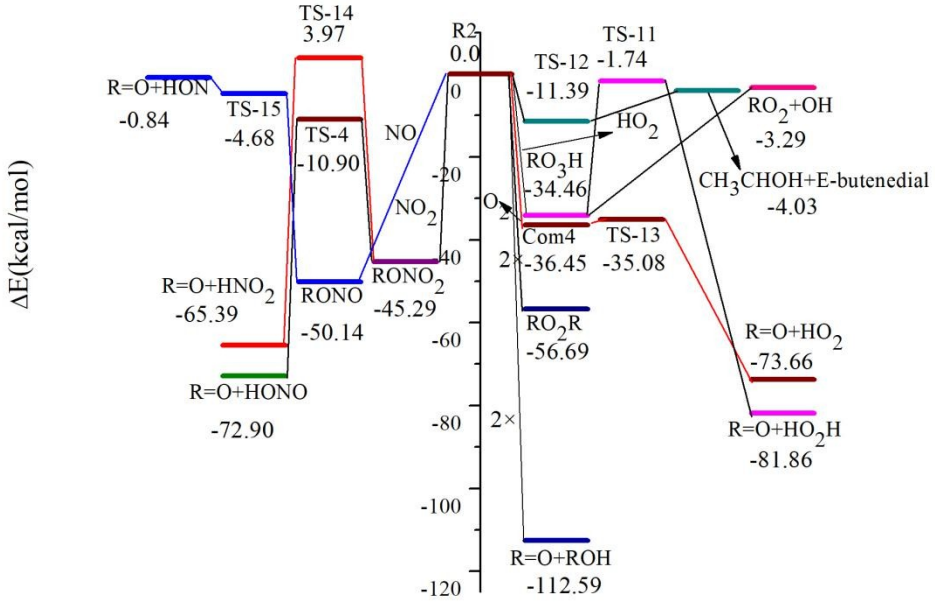

(g)

Figure 2 Potential energy surfaces for all reactions obtained at the BMC-CCSD//M06-2X/6-311G (d, p) level. (a) Hydrogen abstraction paths. (b) C-addition paths. (c) Reaction paths of $CH_3CHOHCHO_2CH$=CHCHO (R1) with NO. (d) Reaction paths of R1 with NO_2. (e) Reaction paths of R1 with HO_2. (f) R1 self-reaction paths. (g) Reaction paths of $CH_3CHOHCHOCH$=CHCHO (R2) with O_2, NO, NO_2, HO_2 and self-reaction.

3.1 Reaction mechanism of hydrogen abstraction

As shown in Figure 2(a), it is a potential energy diagram of hydrogen abstraction of E,E-2,4-hexadienal with OH radical, where the total energy of E,E-2,4-hexadienal and OH radical is set to zero. OH radical can capture hydrogen atom from C1, C2, C3, C4 and C5 of E,E-2,4-hexadienal through HTS1, HTS2, HTS3, HTS4 and HTS5,

respectively. And the energy barriers of HTS1, HTS2, HTS3, HTS4 and HTS5 are -1.03, 1.97, 2.27, 2.49 and 1.77 kcal/mol respectively. Moreover, the corresponding products P1 ($CH_2CH=CHCH=CHCHO+H_2O$), P2 ($CH_3C=CHCH=CHCHO+H_2O$), P3 ($CH_3CH=CCH=CHCHO+H_2O$), P4 ($CH_3CH=CHC=CHCHO+H_2O$), and P5 ($CH_3CH=CHCH=CCHO+H_2O$) are more exothermic 39.81, 9.61, 12.00, 18.52 and 8.39 kcal/mol, respectively. In addition, OH radical can also extract hydrogen atom from -CHO group to generate P6($CH_3CH=CHCH=CHCO+H_2O$) via transition state HTS6 (-2.23 kcal/mol relative to reactants). The formation of P6 is also exothermic 29.97 kcal/mol. The IRC calculation confirms that HTS1 is connected to P1 through complex CR2 and HTS6 is connected to later complex CP through early complex CR1. The pre- and post-reactive complex represent the interaction of OH and H_2O with E,E-2,4-hexadienal, respectively. In fact, hydrogen abstraction from CH_3- and -CHO group are the most important channels compared with hydrogen abstraction from C2, C3, C4 and C5 of E,E-2, 4-hexadienal.

3.2 Reaction mechanism of carbon addition

There are four carbon addition channels. It can be seen that double bond addition of OH radical at C2 and C3 of E,E-2,4-hexadienal would happen though TS1 (-4.36 kcal/mol) and TS2 (-2.04 kcal/mol). Because the energies of TS1 and TS2 are lower than that of the reactants, an entrance complex named Com1 would be formed with the energy of -2.78 kcal/mol. From Com1, OH radical can add to C2 site of E, E-2,4-hexadienal via TS1 to form the intermediate IM1, or to C3 via TS2 with the formation of IM2. TS1 shows that the distance between C2 and oxygen is 2.178 Å.

TS2 is similar to TS1, namely, bond length between C3 and oxygen is 2.047 Å. IRC calculation determines that the connection of TS1 and TS2 is both from Com1 to IM1 and IM2, respectively. And the relative energies of IM1 and IM2 is -42 and -22.65 kcal/mol. In the same way, OH radical can also add at C4 and C5 with IM3 (-27.56 kcal/mol) and IM4 (-37.36 kcal/mol) formation via TS3(-2.63 kcal/mol) and TS4(-2.38 kcal/mol), respectively. IRC calculation confirms TS3 and TS4 connect to IM3 and IM4 through Com2. The distance between C4 and oxygen is 2.072 Å in TS3, and that of TS4 is 2.135 Å. The potential energy surface of carbon addition implies that the intermediate IM1 is the most important adduct for the reaction of E,E-2,4-hexadienal and OH radical. This conclusion can be attributed to the positive inductive effect of the methyl group attached to C2. Colmenar et al. has proposed that a double bond addition of OH radical at C2/C3 of E,E-2,4-hexadienal is the first step for tropospheric degradation.

Theoretically, Vega-Rodriguez et al. studied the reaction mechanism of three unsaturated aldehydes with hydroxyl radical at M05-2X/6-311++G(d, p) level[27]. The sites of OH addition and hydrogen abstraction have been predicted. And branching ratios for addition and abstraction have been also calculated. The results suggested that β carbon atom addition and aldehydic hydrogen abstraction are dominant. According to experimental data, the addition channels become increasingly important when hydrogen on the unsaturated aldehyde is substituted by methyl group. Hence, it is easy to draw a conclusion that the C2 site addition leading to the formation of IM1 is the most important for initial reaction of E,E-2,4-hexadienal with

OH radical.

Under atmospheric conditions, IM1 would combine with oxygen rapidly to generate R1 ($CH_3CHOHCHO_2CH=CHCHO$) with an energy of -44.62 kcal/mol. In the following sections, we will study the detailed reaction mechanism of R1 with NO*x* (NO and NO_2), HO_2 and self-reaction by quantum chemical calculations. Meanwhile, the subsequent degradation pathways of the dominant intermediate R2 ($CH_3CHOHCHOCHCHCHO$) have also been calculated.

3.3 Reaction mechanism of R1 and NO

Figure 2(c) shows the potential energy surface of the reaction of R1 and NO. We set the total energy of R1+NO to zero, and the energies of other species are relative to the reactants. For R1+NO reactions, R1 and NO firstly generate Trans-RO_2NO and Cis-RO_2NO whose energies are -23.06 and -24.29 kcal/mol respectively. They would transform each other via a transition state TS-1 (-21.88 kcal/mol). The two isomers would be decomposed into the product $CH_3CHOHCHOCH=CHCHO$ (RO)+NO_2 (-10.46 kcal/mol) without barrier. Furthermore, RO and NO_2 radicals are combined to generate stable compound $RONO_2$ (-55.07 kcal/mol). For the formation of $RONO_2$, quantum chemical calculations for CH_3O_2+NO and $PhCH_2O_2$+NO assured that $RONO_2$ is formed from the recombination of CH_3O+NO_2 and $PhCH_2O$+NO_2 not from transformation of RO_2NO[28-30]. In this work, a new source of $RONO_2$ containing an aldehyde group in the atmosphere is found. In addition, we have determined two routes from Cis-RO_2NO and Trans-RO_2NO to $CH_3CHOHCOCH=CHCHO$ (R=O) +HONO (-77.33 kcal/mol) by transition states TS-2 (10.59 kcal/mol) and TS-3 (13.92

kcal/mol), respectively. The intermediate $RONO_2$ (-55.07 kcal/mol) can also generate the product R=O+HONO via transition state TS-4 (-18.27 kcal/mol).

3.4 Reaction Mechanism of R1 and NO_2

In the presence of NO_2, R1 and NO_2 combine to generate analogous alkylperoxy nitrates RO_2NO_2 and release 24.33 kcal/mol of energy without any barrier. RO_2NO_2 would be decomposed into $RO+NO_3$ requires an energy of 40.79 kcal/mol, and R=O and HNO_3 can also be generated through TS-5 (7.55 kcal/mol) with a barrier of 31.88 kcal/mol. However, the reaction is highly exothermic 78.09 kcal/mol. Reactions with NO and NO_2 play an important role in losing process of $CH_3CHOHCHO_2CH=CHCHO$. And the peroxynitrates (RO_2NO_2 and $RONO_2$) have been also observed in the experiment. They would contribute to the photochemical smog and have a potential impact on the atmospheric chemistry.

3.5 Reaction Mechanism of R1 and HO_2

Some experimental results have proved that the products of $ROOH+O_2$ are dominant between RO_2 and HO_2 reaction[31-34]. And the formation of OH radical has been directly observed in RO_2 + HO_2 reaction. Hasson et al. analyzed the products for acetyl peroxy ($CH_3C(O)O_2$) and HO_2 reaction with FTIR and HPLC methods and obtained about 0.4 branching ratios of OH radical[35]. Jenkin also received similar results by using the analogous methods[36].

In this work, the triplet and singlet potential energy surfaces (PESs) of the reaction mechanism of R1 and HO_2 are shown in Figure 2(e). It is indicated that R1 and HO_2 primarily form a complex Com3 in the triplet state with the energy of -7.08

kcal/mol. Subsequently, Com3 generates $CH_3CHOHCHOOHCH=CHCHO$ (RO_2H) and triplet O_2 via transition state TS-6 (-4.71 kcal/mol) with a barrier of 2.37 kcal/mol. And this pathway is highly exothermic 23.12 kcal/mol. Thus, the reaction from Com3 to $RO_2H+{}^3O_2$ would be very fast. $PhCH_2O_2H+{}^3O_2$ are dominant products from triplet PES of $PhCH_2O_2+HO_2$ in the Feng et al.'s study at the CCSD(T) level of theory. In $PhCH_2O_2+HO_2$ reaction, the energy of triplet hydrogen-bond complex is -4.99 kcal/mol and the transition state is located at -1.07 kcal/mol with a barrier of 3.92 kcal/mol. The dominant products of $CH_3OOH+{}^3O_2$ and $C_2H_5OOH+{}^3O_2$ from $CH_3O_2+HO_2$ and $C_2H_5O_2+HO_2$ were calculated by Hou et al. at the CCSD(T) level of theory[37,38].

On the singlet state paths, R1 and HO_2 can combine to form $CH_3CHOHCHO_4HCH=CHCHO$ (RO_4H) with the relative energy of -14.21 kcal/mol which is respectively close to the relative energies (-13.14 and -14.46 kcal/mol) of similar structure $C_2H_5O_4H$ from $C_2H_5O_2+HO_2$ and $PhCH_2O_4H$ from $PhCH_2O_2+HO_2$. The first interesting path is that RO_4H decomposes to produce $R=O+HO_2+OH$ (-29.01 kcal/mol) via transition state TS-7 (17.54 kcal/mol). The second one is that it passes TS-8 (16.01kcal/mol) to produce $R=O+HO_3H$ (-58.73 kcal/mol). Moreover, RO_4H can generate $CH_3CHOHCHO_3CHCHCHO$ (RO_3)+OH (10.16 kcal/mol), $RO+HO_3$ (7.67 kcal/mol) and $RO+{}^3O_2+OH$ (9.05 kcal/mol) through heterolytic cleavage, one of $RO+{}^3O_2+OH$ were also reported by Hasson et al. in the $CH_3C(O)O_2+HO_2$ reaction[35]. Therefore, new routes of $CH_3CHOHCHO_2CH=CHCHO$ with HO_2 in this work are described, which help us understand the transformation of HO_2 into OH

295 radical.

296 **3.6 R1 self-reaction mechanism**

297 To our knowledge, some theoretical studies about self-reaction of alkyl peroxy
298 radicals have been carried out, such as CH_3O_2, $CH_3CH_2O_2$, and $PhCH_2O_2$
299 systems[30,39-43]. Ghigo et al. investigated the mechanism of CH_3O_2 self-reaction at
300 the CAS(16,12)-PT2/6-311G(2df,p)//CAS(8,8)-MCSCF/6-311G(d,p) level of theory.
301 They pointed out that the products of $2CH_3O+O_2$ by concerting dissociation from
302 $CH_3O_4CH_3$ are the most favorable. Liang et al. provided a complicated mechanism for
303 CH_3O_2 self-reaction at the CCSD(T)/cc-pVTZ//B3LYP/6311++G(2df,2p) level of
304 theory. From their calculations, the self-reaction of CH_3O_2 mainly occurs on spin-
305 singlet PES. Among these channels, the dominant channels are $2CH_3O+O_2$ and
306 $CH_3OH+CH_2O+O_2$, but the channels leading to $CH_3OOOH+CH_2O$ and
307 $CH_3O+CH_2O+HO_2$ are also energetically favorable. Zhang et al. evaluated reaction
308 mechanism of singlet and triplet self-reaction of $C_2H_5O_2$ radicals at the CCSD(T)/cc-
309 pVDZ//B3LYP/6-311G(2d,2p) level of theory. They suggested that this reaction
310 mainly occurs through singlet oxygen-to-oxygen coupling mechanism with the
311 formation of tetroxide intermediate, and the most dominant product is
312 $C_2H_5O+HO_2+CH_3CHO$. Feng et al. calculated the self-reaction mechanism of
313 $PhCH_2O_2$ by employing cam-B3LYP/dgtzvp and CCSD(T)/CBS methods. Their
314 calculated results indicated that the first channel of forming $PhCH_2O$ and O_2 is the
315 dominant decomposition path of $PhCH_2O_2$ self-reaction, and the second channel of
316 forming PhCHO, $PhCH_2O$ and HO_2 may also be competitive. To sum up, singlet

317 oxygen-to-oxygen coupling mechanism can account for the self-reaction process of
318 peroxy radicals.

319 In this work, we also investigate the self-reaction of peroxy radical including
320 long chain aldehyde group. Figure 2(f) is the PES of the reaction mechanisms of two
321 R1. We set the sum energies of two R1 to be zero and the energies of other species are
322 relative to this energy. The two R1 radicals can combine to form new species RO_4R (-
323 16.81 kcal/mol) without any barrier. The dimer RO_4R structure is similar with
324 $CH_3O_4CH_3$, $C_2H_5O_4C_2H_5$ and $PhCH_2O_4CH_2Ph$. Then RO_4R happens heterolytic
325 cleavage to form $2\times RO+{}^3O_2$ (6.30 kcal/mol). In addition, RO_4R can be also
326 decomposed into RO_3+RO (7.41 kcal/mol). The bond formation and rupture pathway
327 is that RO_4R passes the transition state TS-9 (-1.82 kcal/mol) to form product
328 R=O+RO+HO_2 (-31.76 kcal/mol), with the barrier of 18.63 kcal/mol. In addition, it
329 can also generate the product R=O+RO_3H (-58.16 kcal/mol) via the transition state
330 TS-10 (11.11 kcal/mol), with the barrier of 28.92 kcal/mol. The above calculated
331 results indicated that the forming channel of RO and $^3O_2$ is dominant, and the
332 formation of R=O, RO, and HO_2 may also be competitive, which are close to
333 $PhCH_2O_2$ self-reaction.

334 **3.7 Reaction Mechanism of R2**

335 $CH_3CHOHCHOCH=CHCHO$(R2) is a relatively rich species in above reaction
336 processes. Alkoxy radicals are often formed by the reaction of peroxy radicals with
337 NO, and they strongly influence the production of ozone and SOA in atmospheric
338 conditions[44,45]. Figure 2(g) shows the possible pathways of R2 in the atmosphere,

including reactions with NO, NO_2, O_2, HO_2, self-reaction and decomposition. In the same way, the sum of the energy of reactant is set to zero, and the energies of other species are relative to the energy of reactant. We can find that R2 and HO_2 can quickly combine to form RO_3H (-34.46 kcal/mol) with no barrier. Then RO_3H can generate R=O+HO_2H (-81.86 kcal/mol) through TS-11 (-1.74 kcal/mol) with the energy barrier of 32.72 kcal/mol. And the products of RO_2+OH (-3.29 kcal/mol) can also be obtained by direct dissociation, requiring energy of 31.17 kcal/mol. From the reaction energy barrier point of view, the formations of RO_2+OH and R=O+HO_2H are competitive.

R2 can be decomposed into CH_3CHOH+E-butenedial (-4.03kcal/mol) via TS-12 (-11.39 kcal/mol), which is exothermic 3.20 kcal/mol. Obviously, it is very easy to form the products of CH_3CHOH+E-butenedial, which is also in accordance with Colmenar's conclusion on the degradation mechanism of E,E-2,4-hexadienal and atmospheric oxidants (OH, Cl, and NO_3)[14]. Wu et al. proposed toluene to be the E-butenedial's precursor[46]. And E-butenedial would yield maleic anhydride that may affect environment and human health because it is low volatility organic hazardous air pollutant[47]. And atmospheric chemistry of maleic anhydride have been investigated: photolysis and reaction with OH radical[48,49]. The reaction of R2 and O_2 should be the main path under atmospheric conditions, because the concentration of oxygen in the atmosphere is much higher than that of other active radicals. R2 and O_2 first form complex Com4 with energy of -36.45 kcal/mol. Later, Com4 generates R=O+HO_2 with energy barrier of 1.37 kcal/mol through transition state TS-13 (-35.08 kcal/mol).

Therefore, R=O should be the abundant compound under atmospheric conditions. In addition, two R2 free radicals can form RO_2R (-56.69 kcal/mol) and ROH+R=O (-112.59 kcal/mol) without barrier.

As for the reaction mechanism of R2 and NO_2, R2 and NO_2 firstly combine to form $RONO_2$ without obstacles. This path is exothermic -46.25 kcal/mol. From $RONO_2$, there are two paths. One is to generate R=O+HONO (-72.90 kcal/mol) through the transition state TS-4 (-10.90 kcal/mol); The other is to form R=O+HNO_2 (-65.39 kcal/mol) via transition state TS-14 (3.97 kcal/mol). The barrier heights of TS-4 and TS-14 are 34.39 and 49.26 kcal/mol, respectively. Considering energy barrier, the formation of R=O+HONO is relatively easy. R2 and NO can be mixed to form RONO (-50.14 kcal/mol) without any barrier. The products of R=O+HON (-0.84 kcal/mol) are produced through TS-15 (-4.68 kcal/mol) with an energy barrier of 45.46 kcal/mol.

The above reaction pathways reveal that the product yields depend on the concentration of active radicals such as O_2, NO_x, and HO_2. For example, under atmospheric condition, the concentration of O_2 is very high. Thus, the products R=O+HO_2 account for a substantial part. More importantly, the products of CH_3CHOH+E-butenedial decomposed by the unimolecular reaction of R2 are also dominant.

4. Conclusion

In this paper, the multichannel atmospheric reaction mechanisms of CH_3CH=CHCH=CHCHO+OH have been studied by quantum chemical methods. It is

found that the first pathways are hydrogen abstraction and carbon addition for E, E-2,4-hexadienal initiated by OH radical. The six hydrogen abstraction channels are found, namely, extracting H atom from C1, C2, C3, C4, C5 and C6 of E, E-2,4-hexadienal, respectively. The products of P1 ($CH_2CHCHCHCHCHO+H_2O$), P2 ($CH_3CCHCHCHCHO+H_2O$), P3 ($CH_3CHCCHCHCHO+H_2O$), P4 ($CH_3CHCHCCHCHO+H_2O$), P5 ($CH_3CHCHCHCCHO+H_2O$) and P6 ($CH_3CHCHCHCHCO+H_2O$) would be formed. Of course, on the potential energy surface, hydrogen atom abstraction from C6 is dominant and P6 has the largest branching ratio. There are four carbon addition reaction paths. E,E-2,4-hexadienal and OH radical can add to generate intermediates IM1 ($CH_3CHOHCHCHCHCHO$), IM2 ($CH_3CHCHOHCHCHCHO$), IM3 ($CH_3CHCHCHOHCHCHO$) and IM4 ($CH_3CHCHCHCHOHCHO$) through TS1, TS2, TS3 and TS4, respectively. The potential energy surface reflects that IM1 is the most important intermediate.

IM1 can rapidly combine with oxygen to form R1 ($CH_3CHOHCHO_2CHCHCHO$). Quantum chemical calculations have been used to study the degradation mechanism of R1 with NO, NO_2, HO_2 and self-reaction. R1+NO firstly produces RO and NO_2 radicals, and the potential energy surface forming RO and NO_2 can recombine into $RONO_2$. As for R1+NO_2, we found that the binding of R1+NO_2 to RO_2NO_2 is reversible. Compared with other dissociation pathways (RO+NO_3, R=O+HNO_3), RO_2NO_2 is favorable to return R1+NO_2. The R1+HO_2 reaction can generate $RO_2H+{}^3O_2$ on triplet state energy surface, which is feasible. It can also form RO_4H on the singlet state without barrier and RO is found to be a rich substance. The self-reaction of R1 firstly would occur to form an interesting

406 compound RO_4R. It is found that the most favorable reaction path is the formation of
407 $RO+{}^3O_2$ from RO_4R. As the primary product RO(R2), it may react with O_2, NO, NO_2,
408 H_2O, and self-reaction. The interesting thing is that CH_3CHOH+E-butenedial through
409 the carbon-carbon single bond fracture of R2 are dominant products. In a word, the
410 above studies have established the contribution of E,E-2,4-hexadienal to atmospheric
411 chemistry.

412 **Acknowledgments**

413 This work is supported by the National Natural Science Foundation of China
414 (Nos. 21507027, 21707062, and 41775119).

415 **Reference**

416 [1] M. Jang, R. M. Kamens, Environ. Sci. Technol. **2001**, 35, 3626-3639.
417 [2] A. Mellouki, T. J. Wallington, J. Chen, Chem. Rev. **2015**, 115, 3984-4014.
418 [3] R. Atkinson,J. Arey, Chem. Rev. **2003**, 103, 4605-4638.
419 [4] J. A. Logan, J. Geophys. Res. **1985**, 90, 10463-10482.
420 [5] S. M. Zhou, I. Barnes, T. Zhou, B. Klotz, M. Albu, I. Bejan, T. Benter, Environ.
421 Sci. Technol. **2006**, 40, 5415-5421.
422 [6] S. Y. Wang, L. Du, J. Q. Zhu, N. T. Tsona, S. J. Liu, Y. F. Wang, M. F. Ge, W. X.
423 Wang, J. Phys. Chem. A. **2018**, 122, 1600-1611.
424 [7] W. P. L. Carter, J. Air Waste Manage. **1994**, 44, 881-899.
425 [8] R. Ballesteros, E. Monedero, J. Guillen-Flores, Atmos. Environ. **2011**, 45, 2690-
426 2698.
427 [9] A. C. Heiden, K. Kobel, C. Langebartels, G. Schuh-Thomas, J. Wildt, J. Atmos.
428 Chem. **2003**, 45, 143-172.

[10] J. A. de Gouw, C. J. Howard, T. G. Custer, R. Fall. Geophys. Res. Lett. **1999**, 26, 811-814.

[11] J. Zhao, N. P. Levitt, R.Y. Zhang, Geophys. Res. Lett. **2005**, 32, L09802.

[12] M. P. O'Connor, J. C. Wenger, A. Mellouki, K. Wirtz, A. Muńoz, Phys. Chem. Chem. Phys. **2006**, 8, 5236-5246.

[13] I. Colmenar, P. Martín, B. Cabañas, S. Salgado, E. Martínez, Atmos. Environ. **2014**, 99, 159-167.

[14] I. Colmenar, P. Martín, B. Cabañas, S. Salgado, E. Martínez, Atmos. Environ. **2018**, 176, 188-200.

[15] J. J. Orlando, G. S. Tyndall, Chem. Soc. Rev. **2012**, 41, 6294-6317.

[16] Y. Zhao, D. G. Truhlar, Theor. Chem. Acc. **2008**, 120, 215-241.

[17] A. D. McLean, G. S. Chandler, J. Chem. Phys. **1980**, 72, 5639-5648.

[18] M. H. Keshavarz, K. Esmailpour, M. Zamani, A. G. Roknabadi, Propell. Explos. Pyrot. **2015**, 40, 886-891.

[19] S. R. Hashemi, V. Saheb, Comput. Theor. Chem. **2017**, 1119, 59-64.

[20] F. Y. Bai, S. Ni, Y. Z. Tang, X. M. Pan, Z. Zhao, Sci. Total. Environ. **2020**, 699, 134-190.

[21] C. Gonzalez, H. B. Schlegel, J. Chem. Phys. **1989**, 90, 2154-2161.

[22] C. Gonzalez, H. B. Schlegel, J. Phys. Chem. **1990**, 94, 5523-5527.

[23] B. J. Lynch, Y. Zhao, D. G. Truhlar, J. Phys. Chem. A. **2005**, 109, 1643-1649.

[24] Y. M. Ji, Y. P. Gao, G. Y. Li, T. C. An, Atmos. Environ. **2012**, 54, 288-295.

[25] Y. M. Ji, H. H. Wang, J. Y. Chen, G. Y. Li, T. C. An, X. L. Zhao, J. Phys. Chem. A. **2015**, 119, 11376-11383.

452 [26] M. J. Frisch, G. W. Trucks, H. B. Schlegel, G. E. Scuseria, M. A. Robb, J. R.
453 Cheeseman, J. A. Montgomery, Jr. T. Vreven, K. N. Kudin, J. C. Burant, J. M. Millam,
454 S. S. Iyengar, J. Tomasi, V. Barone, B. Mennucci, M. Cossi, G. Scalmani, N. Rega,
455 G.A. Petersson, H. Nakatsuji, M. Hada, M. Ehara, K.Toyota, R. Fukuda, J. Hasegawa,
456 M. Ishida, T. Nakajima, Y. Honda, O. Kitao, H. Nakai, M. Klene, X. Li, J. E. Knox, H.
457 P. Hratchian, J. B. Cross, C. Adamo, J. Jaramillo, R. Gomperts, R. E. Stratmann, O.
458 Yazyev, A. J. Austin, R. Cammi, C. Pomelli, J. W. Ochterski, P. Y. Ayala, K.
459 Morokuma, G. A. Voth, P. Salvador, J. J. Dannenberg, V. G. Zakrzewski, S. Dapprich,
460 A. D. Daniels, M. C. Strain, O. Farkas, D. K. Malick, A. D. Rabuck, K. Raghavachari,
461 J. B. Foresman, J. V. Ortiz, Q. Cui, A. G. Baboul, S. Clifford, J. Cioslowski, B. B.
462 Stefanov, G. Liu, A. Liashenko, P. Piskorz, I. Komaromi, R. L.Martin, D. J. Fox, T.
463 Keith, M. A. Al-Laham, C. Y. Peng, A. Nanayakkara, M. Challacombe, P. M. W. Gill,
464 B. Johnson, W. Chen, M. W. Wong, C. Gonzalez, J. A. Pople, Gaussian Inc,
465 Pittsburgh, PA, **2010**.
466 [27] A. Vega-Rodriguez, J. R. Alvarez-Idaboy, Phys. Chem. Chem. Phys. **2009**, 11,
467 7649-7658.
468 [28] H. T. Nguyen, T. V. -T. Mai, L. K. Huynh, Comput. Theor. Chem. **2017**, 1113,
469 14-23.
470 [29] A. M. Launder, J. Agarwal, H. F. Schaefer III, J. Chem. Phys. **2015**, 143, 234-
471 302.
472 [30] B. Feng, C. H. Sun, S. W. Zhang, Atmos. Environ. **2019**, 201, 18-27.
473 [31] T. J. Wallington, S. M. Japar, Chem. Phys. Lett. **1990**, 167, 513-518.

[32] T. J. Wallington, S. M. Japar, Chem. Phys. Lett. **1990**, 166, 495-499.

[33] P. D. Lightfoot, P. Roussel, F. Caralp, R. Lesclaux, J. Chem. Soc. Faraday Trans. **1991**, 87, 3213-3220.

[34] M. Spittler, I. Barnes, K. H. Becker, T. J. Wallington, Chem. Phys. Lett. **2000**, 321, 57-61.

[35] A. S. Hasson, G. S. Tyndall, J. J. Orlando, J. Phys. Chem. **2004**, 108, 5979–5989.

[36] M. E. Jenkin, M. D. Hurley, T. J. Wallington, Phys. Chem. Chem. Phys. **2007**, 9, 3149-3162

[37] H. Hou, B. S. Wang, J. Phys. Chem. A. **2005**, 109, 451-460.

[38] H. Hou, J. C. Li, X. L. Song, B. S. Wang, J. Phys. Chem. A. **2005**, 109, 11206-11212.

[39] G. Ghigo, A. Maranzana, G. Tonachini, J. Chem. Phys. **2003**, 118, 10575-10583.

[40] T. S. Dibble, Atmos. Environ. **2008**, 42, 5837-5848.

[41] Y. N. Liang, J. Li, Q. D. Wang, F. Wang, X. Y. Li, J. Phys. Chem. A. **2011**, 115, 13534-13541.

[42] P. Zhang, W. L. Wang, T. L. Zhang, L. Chen, Y. M. Du, C. Y. Li, J. Lu, J. Phys. Chem. A. **2012**, 116, 4610-4620.

[43] B. Feng, Y. Shu, S. W. Zhang, Struct. Chem. **2020**, 31, 123-132.

[44] T. S. Dibble, J. J. Chai, Advan. In Atmos. Chem. **2017**, 185-269.

[45] R. Atkinson, W. P. L. Carter, J. Atmos. Chem. **1991**, 13, 195-210.

[46] R. R. Wu, S. S. Pan, Y. Li, L. M. Wang, J. Phys. Chem. A. **2014**, 118, 4533-4547.

[47] D. Grosjean, J. Air. Waste. Manage. Assoc. **1990**, 40, 1664-1669.

[48] A. Chattopadhyay, V. C. Papadimitriou, P. Marshall, J. B. Burkholder, Int. J.

Chem. Kinet. **2020**, 1-9.

[49] P. Marshall, V. C. Papadimitriou, D. K. Papanastasiou, J. M. Roberts, J. B. Burkholder, J. Photoch. Photobio. A. **2019**, 382, 111953.